Articles in PresS. Am J Physiol Regul Integr Comp Physiol (March 23, 2016). doi:10.1152/ajpregu.00309.2015

Cardiac hypertrophy and decreased high-density lipoprotein cholesterol in Lrig3-deficient mice

Martin Hellström[1]*[#], Madelene Ericsson[2]*, Bengt Johansson[3], Mahmood Faraz[1], Fredrick Anderson[2], Roger Henriksson[1,4], Stefan K Nilsson[2#], and Håkan Hedman[1]

*Contributed equally to this work.

[#]Shared corresponding authorship.

[1]Department of Radiation Sciences, Oncology, Umeå University, SE-90187 Umeå, Sweden

[2]Department of Medical Biosciences, Physiological Chemistry, Umeå University, SE-90187 Umeå, Sweden

[3]Department of Public Health and Clinical Medicine, Medicine, Umeå University, SE-90187 Umeå, Sweden

[4]Regional Cancer Center Stockholm/Gotland, Box 6909, SE-10239 Stockholm, Sweden

Running head: Lrig3-deficiency, a risk factor for cardiovascular disease?

Address for correspondence:

Martin Hellström

Department of Radiation Sciences, Oncology, Umeå University, SE-90187 Umeå, Sweden

Phone: +46 (0) 90 785 7875

Fax: +46 (0) 90 785 2031

E-mail: martin.hellstrom@onkologi.umu.se

and

Stefan K. Nilsson

Department of Medical Biosciences, Physiological Chemistry, Building 6M 3tr, Umeå University, SE-90187 Umeå, Sweden

Phone: +46 (0)70 578 1768

E-mail: Stefan.k.nilsson@umu.se

Abstract:

Genetic factors confer risk for cardiovascular disease. Recently, large genome-wide population studies have shown associations between genomic loci close to *LRIG3* and heart failure and plasma high-density lipoprotein (HDL) cholesterol level. Here, we ablated *Lrig3* in mice and investigated the importance of *Lrig3* for heart function and plasma lipid levels. Quantitative reverse transcription polymerase chain reaction (RT-PCR) was used to analyze *Lrig3* expression in the hearts of wild-type and *Lrig3*-deficient mice. In addition, molecular, physiological, and functional parameters such as organ weights, heart rate, blood pressure, heart structure and function, gene expression in the heart, and plasma insulin, glucose and lipid levels were evaluated. The *Lrig3*-deficient mice were smaller than the wild-type mice but otherwise appeared grossly normal. *Lrig3* was expressed at detectable but relatively low levels in adult mouse hearts. At nine months of age, ad libitum fed *Lrig3*-deficient mice had lower insulin levels than wild-type mice. At 12 months of age, *Lrig3*-deficient mice exhibited increased blood pressure, and the *Lrig3*-deficient female mice displayed signs of cardiac hypertrophy as assessed by echocardiography, heart-to-body-weight ratio, and expression of the cardiac hypertrophy marker gene *Nppa*. Additionally, *Lrig3*-deficient mice had reduced plasma HDL-cholesterol and free glycerol. These findings in mice complement the human epidemiological results and suggest that *Lrig3* may influence heart function and plasma lipid levels in mice and humans.

Keywords: Heart, Lrig3, Hypertrophy, Mice, Cholesterol

Introduction:

Many factors contribute to the risk of cardiovascular disease. Recently, a large meta-analysis of 4 prospective cohort-studies found a single-nucleotide polymorphism (SNP) at a genomic locus close (6.3 kb) to the leucine-rich repeats and immunoglobulin-like domains 3 (*LRIG3*) gene that has a strong association with development of heart failure (37). Another study identified another SNP close (53 kb) to *LRIG3* that is linked to plasma high-density lipoprotein (HDL) cholesterol level (25). Low HDL-cholesterol is an independent risk factor for developing atherosclerosis (4). LRIG3 is a member of a family of transmembrane proteins that also includes LRIG1 and LRIG2 (9). LRIG1 negatively regulates various receptor tyrosine kinases, including all of the epidermal growth factor receptor (EGFR) family members (11, 19), rearranged during transfection (RET) (20), hepatocyte growth factor receptor (MET) (36), and platelet-derived growth factor receptor alpha (PDGFRA) (34). Less is known about the molecular functions of LRIG2 and LRIG3. Recently, however, it was suggested that LRIG3 opposes the function of LRIG1 (33). All three LRIG family members are prognostic markers for different types of cancer (10, 13, 14, 18, 23, 24, 26, 35, 39). To evaluate the developmental and physiological functions of the LRIG proteins, our group and others have deleted the different *Lrig* genes in mice. *Lrig1*-deficient mice postnatally develop macroscopic psoriasis-like skin lesions on the tail, ears, and face (38). This phenotype is accompanied by hyperproliferation and expansion of epidermal and intestinal stem cells (16, 17, 32, 42). In addition, the *Lrig1*-deficient mice show an increased incidence of intestinal adenomas (32, 42), and have an abnormal corneal stem cell phenotype (27). *Lrig2*-deficient mice are protected against PDGFB-induced gliomas but also have an increased rate of idiopathic spontaneous mortality (34), and they show hearing defects (6). *Lrig3*-deficient mice exhibit craniofacial and inner ear defects (1). To our knowledge, cardiac function and plasma lipid levels have not been studied in any *Lrig*-deficient mouse strain, to date.

The present study investigated whether *Lrig3* is important for heart function and for regulating plasma cholesterol level in mice. We generated *Lrig3*-deficient mice and compared their heart function and plasma lipid levels to those in wild-type mice.

Materials and methods:

Animals and tissues

All mice were housed and maintained and the experiments performed in accordance with the European Communities Council Directive (86/609/EEC). The experimental protocols were approved by the Regional Ethics Committee of Umeå University, Umeå, Sweden (registration nos. A5-2010 and A105-2011).

Construction of the *Lrig3* targeting vector and generation of mice with floxed (B6.129-*Lrig3*^{tm1Hhed}) and deleted (B6.129-*Lrig3*$^{tm1.1Hhed}$) *Lrig3* alleles were performed at Ozgene (Bentley DC, WA, Australia) using the same protocol as previously described for the generation of *Lrig2*-deficient mice (34). A schematic drawing of the *Lrig3* wild-type, conditional, and disrupted alleles is shown in Figure 1A. The *Lrig3E1*-deleted allele was transferred to a pure mouse genetic background by backcrossing onto the C57BL/6 background for 10 generations. In total, 11 female wild-type mice (hereafter called WT), 13 male WT, 12 female *Lrig3*-deficient (KO), and 11 male KO were included in the study. The animals were kept in standard mouse cages with free access to standard rodent chow (Special Diets Services, #801730) and water with a light period from 6:00 a.m. to 6:00 p.m. Physiological measurements and blood sampling were performed at 6, 9 and 12 months of age. After the final measurements, the 12-month-old animals were euthanized by cervical

dislocation and weighed. The heart, lungs, liver, spleen, and right tibia were collected and weighed immediately after death. The lungs, liver, and spleen were transferred to 4% buffered formalin or RNAlater (Life Technologies, Stockholm, Sweden). The atria, left ventricle, and right ventricle were weighed separately, divided into parts, and then transferred to 4% buffered formalin or RNAlater or snap-frozen in N_2 (l). The length of the right tibia was measured using a digital Vernier caliper.

Genotyping

Genotyping was performed twice for each animal, at weaning and, to confirm the genotype, at the end of the experiment, by PCR as previously described for *Lrig2* using the primers 5' – GCTGGAGCCTTGTTATTGTCAC –3' and 5'– CGAGGCTGATGGTCTGCTA – 3'. The PCR products (800 bp for the WT and 350 bp for the KO) were separated and visualized using analytical agarose gel electrophoresis.

Antibodies and immunoblotting

The rabbit polyclonal antibody mLrig3-207 against the synthetic peptide CGTFGKPLRRPHLDA (single-letter amino acid code) in the cytosolic tail of mouse Lrig3 was developed and affinity-purified in collaboration with Agrisera AB (Vännäs, Sweden) as previously described for LRIG1 (28). Mouse anti-actin antibody was purchased from Millipore AB (Solna, Sweden). Horseradish peroxidase-conjugated secondary antibodies were purchased from GE Healthcare (Uppsala, Sweden). The skin from newborn mice was dissected, followed by lysis in modified RIPA buffer [50 mM Tris-HCl, pH 7.4, 1% Triton X-100, 0.2% sodium deoxycholate, 0.2% sodium-dodecyl-sulfate (SDS), 1 mM sodium ethylene diamine tetra acetate, 1 mM phenylmethylsulfonylfluoride, freshly added Complete Mini protease inhibitor cocktail (Roche Diagnostics Scandinavia AB, Stockholm, Sweden)]. The

samples were incubated on ice for 30 min. After a brief homogenization, the samples were incubated for another hour on a shaker at 4°C and then centrifuged at 20,900 x *g* for 15 min. The supernatants were collected, and protein concentrations were determined using a BCA protein assay (Pierce Biotechnology Inc., Rockford, IL, USA). Equal amounts of proteins were separated by 3-8% gradient Tris-acetate poly-acryl-amide gel electrophoresis (NuPAGE, Life Technologies) and analyzed using Western blotting. Bound primary antibodies were detected using horseradish peroxidase-conjugated secondary antibodies. The antibody-specific protein bands were visualized using ECL advanced reagent (GE Healthcare).

Quantitative real-time RT-PCR

The RNA was prepared from the left ventricle using the High Pure RNA Paraffin kit (Roche Diagnostics Scandinavia AB) followed by digestion of contaminating DNA using the TURBO DNA-free kit (Life Technologies) according to the manufacturers' instructions. Quantitative reverse transcription (RT)-PCR was performed as previously described (9) using the qScript 1-Step qRT-PCR kit (Quanta Biosciences, Gaithersburg, MD, USA) according to the manufacturer's instructions on a CFX96 Real-Time System C1000 Thermal Cycler. RT-PCR parameters were as follows: 50°C for 10 min, 95°C for 5 min, and 45 cycles of 95°C for 15 sec and 60°C for 30 sec. The following TaqMan gene expression assays were purchased from Applied Biosystems (Life Technologies Europe BV): *Acta1* (actin, alpha 1, skeletal muscle) (Mm00808218_g1), *Nppa* (natriuretic peptide type A, also called atrial natriuretic peptide, ANP, or atrial natriuretic factor, ANF) (Mm01255747_g1), *Gata4* (GATA binding protein 4) (Mm00484689_m1), and *Myh7b* (myosin, heavy chain 7B, cardiac muscle, beta) (Mm01249941_m1). The *Lrig3* and *Rn18s* (also called *18S rRNA*) primer and probe sets have been described previously (9, 29). All mRNA values were normalized against the corresponding *Rn18s* level in the respective sample. To measure *Lrig3* expression in the heart,

the specific mRNA/*Rn18s* ratios were further normalized to the corresponding ratio using QPCR Mouse Reference Total RNA (Agilent Technologies, Santa Clara, CA, USA).

Blood pressure and heart rate measurements

Blood pressure and heart rate were measured using a BP-2000 blood pressure analysis system (Visitech Systems, Inc., Apex, NC, USA) according to the manufacturer's instructions. In short, the animals were placed in a specimen holder on a preheated platform set to 37°C. The tail of each animal was inserted through a tail cuff, placed in the tail slot and secured with a piece of tape. The system performed 10 measurements in each set and also rejected measurements that did not fulfill certain criteria (pulse amplitude, movement) by default. For better reliability and reproducibility, the animals were subjected to one set of measurements daily for 5 days prior to the experimental measurements. The experimental measurements were then performed daily for 5 consecutive days between 7:30 and 12:00 a.m. Each day, the experimental measurements were preceded by one set of preliminary measurements to allow the animals to become accustomed to the holder. For mice with fewer than 5 approved experimental measurements in the first set, a second set was performed resulting in five to ten approved experimental measurements for each animal daily.

High-frequency echocardiography

Cardiac structure and function were evaluated in 21 male and 19 female mice at 6 and 12 months of age using transthoracic, high-frequency echocardiography (Vevo 2100, Visual Sonics, Toronto, ON, Canada). The examination was performed during light isoflurane anesthesia (1.0-2.0% in 800 mL/min O_2) (Baxter Medical AB, Kista, Sweden). The level of anesthesia was adjusted to keep the respiration rate at 90-110 breaths per minute. The images

were acquired using a 55-MHz transducer (Visual Sonics). A detailed protocol for image acquisition was previously described (3). Left ventricular volumes were determined with a Simpson's rule reconstruction.

Plasma measurements

Venous blood samples were collected during an *ad libitum* feeding state at 10.00 a.m. in EDTA-coated capillaries (Greiner Bio-One GmbH, Kremsmünster, Austria). Plasma was collected after 10 min centrifugation at 2,000 x *g* and 4°C. The plasma lipids were measured using size-exclusion HPLC as described elsewhere (30). Plasma insulin and glucose levels in nine months old mice were determined using mouse insulin ELISA (Mercodia, Uppsala, Sweden) and glucose assay kit (MAK013-1KT, Sigma-Aldrich, MO, US), respectively, according to the manufacturers´ instructions.

Histochemistry

Formalin-fixed and paraffin-embedded tissues from the left ventricles of female mice were cross-sectioned in 5-µm-thick serial sections using a HM355S rotary microtome (MICROM International GmbH, Walldorf, Germany).

To visualize endothelium, slides were deparaffinized, rehydrated and incubated with a solution of 3% H_2O_2 in methanol for 20 min, washed in phosphate buffered saline (PBS, pH7.4), and incubated with Proteinase K (S3020, DAKO) for 5 min. All slides were then washed in PBS, put in a protein block solution (X0909, DAKO) for 10 min and incubated with a factor VIII antibody (Von Willebrand factor, A0082, DAKO) at 4°C overnight. After washing in PBS all slides were incubated with Envision HRP Rabbit (K4003, DAKO) for 30

min, washed in PBS and incubated for 5 min in a solution of 3´-diaminobenzidine (DAB, BDB2004, Biocare Medical). Following washing, Mayers hematoxylin was used as counter-staining. Finally, the sections were dehydrated and cover-slipped. The stained sections were evaluated blindly by two of the authors (MH and ME). Cardiomyocyte nuclei and endothelial cell nuclei (defined as nucleus staining that colocalized with Factor VIII staining) were counted in 10 squares á 100x100 µm (NIS Elements AR3.4, Nikon, Japan).

The collagen content was evaluated on sections stained with eosin or Van Gieson's stain and counterstained with Weigert's hematoxylin, and evaluated blindly by two of the authors (MH and BJ). The occurrence of collagen in the myocardial tissue (vessels excluded) was determined in each Van Gieson-stained specimen using a semiquantitative grading scale: absent (0), scarce (+), moderate (++) and abundant (+++).

Statistics

For the statistical analysis, the SPSS statistical analysis package (IBM Statistics SPSS, v 21.0, Chicago, IL, USA) was used. The data were expressed as the mean ± standard deviation (SD). Data were assessed for normality. The different groups (WT versus KO, female WT *versus* KO, and male WT *versus* KO) were compared using one-way ANOVA (Tukey's *post-hoc* test) and Student's *t*-test. For echocardiographic measurements, two-way ANOVA was used for main effect analysis. Mann-Whitney *U*-test was used to compare collagen occurrence. Plasma lipoprotein profiles were compared using generalized estimating equations. The null hypothesis was rejected for p-values < 0.05.

Results:

Lrig3 expression in the heart

Lrig3 expression was analyzed using quantitative RT-PCR. This analysis showed that the *Lrig3* expression level in the left ventricle of 12-month-old female mice corresponded to 9.7% (S.D. ±2.4%, n=11) of the level in the QPCR Mouse Reference Total RNA.

General mouse characteristics

An *Lrig3* KO allele (*Lrig3*$^{tm1.1Hhed}$) was generated by ablation of exon 1, including the predicted ATG start codon, through homologous and Cre recombinase-mediated recombination (Fig. 1A). The KO mice (B6.129-*Lrig3*$^{tm1.1Hhed}$) expressed no detectable Lrig3 full-length protein in skin as analyzed by Western blotting (Fig. 1B). Similarly, *Lrig3* expression was not detected in the KO mouse hearts by quantitative RT-PCR using a probe that spanned the junction between exon 1 and 2 (data not shown). Some of the KO mice, when stressed, were running in circles as previously reported for another *Lrig3*-deficient mouse strain (1). A total of 45 KO and WT mice of both genders were included in the study. Two female KO mice died between 6 and 12 months of age and were excluded from the study. One of the deceased mice had an abdominal tumor, and the other died from unknown cause. At 12 months of age, the majority of mice appeared healthy without obvious macroscopic defects. However, two female KO mice exhibited rectal bleeding and an abdominal tumor was found in one of them upon necropsy. In addition, one male KO mouse had tumorous changes in the liver.

At 12 months, both the female and male KO mice were significantly smaller than the corresponding WT mice as measured by body weight or right tibia length (Table 1). For the

female mice, the left ventricle/body weight ratio was significantly higher for the KO than the WT mice. The body and tissue weights for each group are shown in Table 1.

Microscopic examination of left ventricle sections revealed no apparent differences in morphology between KO (n=9) and WT (n=10) mice (Table 2). The adventitias of intramyocardial vessels were clearly stained for collagen but overall the staining was scarce, mainly detected in the endocardium (Fig 2).
There were no statistically differences in endothelial cell or cardiomyocyte nuclei count, or their ratio, between KO and WT mice (Table 2).

Heart rate and blood pressure

Heart rate and blood pressure were measured in the mice at 6 and 12 months of age. The numbers of heart rate and blood pressure measurements were between 37 and 50 for each mouse. At 6 months of age, the male KO mice had a higher heart rate than their WT counterparts (Table 3). At 12 months of age, KO mice showed a small but significant increase in blood pressure compared with WT mice, 109.7 mm Hg versus 105.6 mm Hg (Table 4).

High-frequency echocardiography

At 6 months of age, the left ventricular diastolic inner diameter was smaller for the female and male KO mice than that of the respective WT mice (Table 5). No other differences between the KO and WT animals were observed by echocardiography at this age.
At 12 months, the female KO mice displayed thicker left ventricular septal and posterior walls and reduced stroke volume with a resulting lower cardiac output than the female WT mice (Table 6).

Gene expression in the female hearts

Because the female KO mice showed signs of cardiac hypertrophy, the expression of a series of fetal/cardiac hypertrophy marker genes was analyzed in left ventricles of 12-month-old female mice using quantitative RT-PCR (Fig. 3). In the female *Lrig3* KO mice, *Nppa* expression was increased by 53% (p=0.012) compared to the female WT mice. Expression of *Gata4*, *Myh7b,* or *Acta1* did not differ between the KO and WT mice.

Plasma lipids, insulin and glucose levels

To investigate the relationship between the *Lrig3* genotype and plasma lipid levels, plasma from 12-month-old KO and WT mice were collected and individually analyzed using size-exclusion HPLC for triglycerides and cholesterol (Fig. 4A-D). At 12 months, KO mice had significantly lower HDL-cholesterol and free glycerol than WT mice (Table 7). HDL-cholesterol was reduced by 12% and 9% in KO female and male mice, respectively, whereas free glycerol was reduced, by 22%, in male KO mice only (Table 7). Given the metabolic relationship between plasma lipids and glucose, we also investigated insulin and glucose levels. At 9 months of age, KO mice fed chow *ad libitum* showed lower plasma insulin levels than WT mice (Table 8).

Discussion

In the present study, we investigated whether *Lrig3* gene status affects heart function and development and plasma lipid levels in mice. Echocardiography revealed that 12-month-old female KO mice had increased left ventricular wall thickness, a cardinal feature of cardiac hypertrophy. There were no differences in heart weight or cardiac morphology between mice of the different genotypes, but because the KO mice were smaller, their left ventricle/body weight ratio was increased compared with WT mice. These results therefore could indicate a

hypertrophic process with impaired cardiac function in female KO mice. Arterial hypertension is a cardiovascular risk factor in humans and is known to cause left ventricular hypertrophy. At 12 months of age, KO mice had higher blood pressure than WT mice. Thus, the cardiac hypertrophy observed could have been the result of pressure overload. The increased heart rate and reduced left ventricular internal diameter in male KO vs. WT mice at 6 months of age were intriguing and could indicate altered heart function in these mice, too, although echocardiography did not reveal any remaining abnormalities in male KO mice at 12 months. Female KO mice expressed increased levels of the cardiac hypertrophy marker gene *Nppa*, suggesting that the observed cardiac hypertrophy in the *Lrig3*-deficient mice was pathological rather than physiological (22).

We observed significantly lower plasma HDL-cholesterol in *Lrig3* KO mice compared to WT mice. This decrease is intriguing because of the previously demonstrated association between HDL-cholesterol level and a SNP in the *LRIG3* region in humans (25). Additionally, in male mice, a reduction in plasma free glycerol was seen. Plasma free glycerol derives from adipose tissue lipolysis of intracellular triglycerides and could reflect differences in the amount of adipose tissue. Plasma insulin levels in 9 months old KO mice were lower than in WT mice. Rodents are known to develop insulin resistance in response to increased fat mass. Thus, a possible explanation for the reduced insulin levels in KO mice could be the lower body weight of the KO mice compared to WT (31). Additionally, in the present study, the blood samples were collected during an *ad libitum* feeding state, which might have contributed to a relatively high intra-group variability for glucose, insulin and VLDL-triglycerides. Although HDL-cholesterol is not affected much by nutritional status, VLDL-triglycerides and non HDL-cholesterol are affected postprandial. Therefore, whereas our findings link *Lrig3* to HDL-cholesterol, possible associations between *Lrig3* and other plasma lipids, glucose and insulin levels, may need new studies of larger series of animals under nutritional control and

challenge, to be revealed. In contrast to humans, mice lack the central cholesteryl ester transfer protein (CETP), which is responsible for HDL re-modulation, transferring cholesterol between HDL and VLDL and transferring triglycerides in the opposite direction (7). Thus, observations regarding HDL- and VLDL-cholesterol levels in mice cannot be directly translated to humans. Nevertheless, the *Lrig3* KO phenotype described here is in line with the human epidemiological studies and suggests that *Lrig3* may regulate cholesterol metabolism in both mice and humans. Further exploration of the function of *Lrig3* in mice expressing CETP and in mice susceptible to atherosclerosis could add important insights regarding the regulation of lipid metabolism, atherosclerosis, and cardiovascular disease in humans.

The Lrig3 KO phenotype differed between male and female mice. Signs of cardiac hypertrophy and reduced plasma cholesterol were more pronounced in female than in male mice, whereas male, but not female, KO mice showed an increased heart rate compared to the corresponding WT mice at 6 months of age. The reason for the sex differences in the observed *Lrig3* phenotype is not known. However, the male and female cardiovascular systems respond differently to aging and hormonal levels (5) and one possible explanation for the sex-specific KO phenotype is that *Lrig3* regulates estrogen levels and/or estrogen signaling pathways, thereby protecting against cardiac hypertrophy and changes in plasma lipid levels. Conversely, estrogen may regulate *Lrig3*, which in turn could have cardioprotective and plasma cholesterol-regulating effects through unknown mechanisms. In this regard, it is notable that *LRIG1* expression is regulated by estrogen and androgens in breast and prostate cancer cells, respectively (18, 41). However, whether *Lrig3* expression is also regulated by sex steroid hormones is not known.

Lrig3 was discovered by our group in 2004, but its function remains largely unknown. In addition to the associations between genomic variants of the *LRIG3* region and heart failure and plasma HDL-cholesterol level, LRIG3 protein expression is associated with patient

353 prognosis in astrocytic cancer (10) and adenocarcinoma of the uterine cervix (26). The latter
354 supports the idea that LRIG3 might interact with growth factor receptors, which are known
355 drivers of human cancer (12). Recently, LRIG3 was suggested to oppose the function of
356 LRIG1 (33), which is a well-established regulator of growth factor signaling. The notion that
357 LRIG3 interacts with growth factor receptors is also supported by Zhao *et al.* ((43)), who
358 showed that LRIG3 interacts with FGF and Wnt signaling in *Xenopus laevis* during embryo
359 development. The EGFR family members, EGFR, ERBB2, ERBB3 and ERBB4, are
360 important both during embryonic cardiovascular development and for mature cardiac
361 function. EGFR seems to inhibit the differentiation of cardiomyocytes *in vitro*, whereas
362 deletion of *Erbb2* or *Erbb4* in mice is lethal due to developmental heart defects (8, 21).
363 Trastuzumab, an antibody against ERBB2 that is used in cancer treatment, is cardiotoxic and
364 sometimes causes left ventricular systolic dysfunction as a side effect (40). Like Lrig1, Lrig3
365 interacts with the EGFR-family members *in vitro* (2), but the relevance *in vivo* of this
366 potential interaction is still unclear. The relatively low expression of *Lrig3* that was observed
367 in the heart is consistent with an earlier report and public expression data sets showing scarce
368 *Lrig3* expression in hearts from mouse embryos ((15), GenePaint, www.genepaint.org, March
369 1, 2013) and little to no LRIG3 immunoreactivity in adult human hearts (The Human Protein
370 Atlas, version 11.0, www.proteinatlas.org, March 1, 2013). Thus, although it seems plausible
371 that our observed *Lrig3* KO phenotype was the consequence of deregulated growth factor
372 signaling, the identity of the growth factor receptors that would be affected or in what tissues
373 and cell types this regulation would be important are not known. Both male and female KO-
374 mice were smaller than the corresponding WT mice. Reduced body weight could also be due
375 to malnutrition, possibly because of anatomical defects. Abraira *et al.* ((1)) described
376 craniofacial defects in their Lrig3-deficient mice, however, no apparent craniofacial defects

were detected in our Lrig3-deficient mouse strain, and no obvious signs on reduced food intake were seen.

Perspectives and Significance

Recently, large human genome-wide population studies have shown associations between genomic loci close to *LRIG3*, heart failure, and plasma HDL-cholesterol level. Here, we report that *Lrig3*-deficient female mice developed signs of cardiac hypertrophy, and Lrig3-deficient mice also showed reduced plasma HDL-cholesterol and free glycerol levels at 12 months of age. Our findings in mice complement the human epidemiological studies and suggest that *Lrig3* may influence heart function and plasma lipid levels in mice and humans. Further studies are needed to determine mechanistically how *Lrig3* affects cardiac function and plasma lipids. Such knowledge may eventually be translated into tools for better prediction of cardiovascular disease risk and possibly for novel cardiovascular disease treatment paradigms.

Acknowledgments

We thank Charlotte Nordström, Annika Holmberg, and Yvonne Jonsson for technical help. This work was supported by grants from the European Union FP7 CarTarDis consortium, the Swedish Research Council, the Swedish Cancer Society, the Heart Foundation of Northern Sweden, the Lion's Cancer Research Foundation at Umeå University, the Cancer Research Foundation in Northern Sweden, and through a regional agreement between Umeå University and Västerbotten County Council (ALF).

References

1. **Abraira VE, Del Rio T, Tucker AF, Slonimsky J, Keirnes HL, and Goodrich LV.** Cross-repressive interactions between Lrig3 and netrin 1 shape the architecture of the inner ear. In: *Development*. England, 2008, p. 4091-4099.

2. **Abraira VE, Satoh T, Fekete DM, and Goodrich LV.** Vertebrate Lrig3-ErbB interactions occur in vitro but are unlikely to play a role in Lrig3-dependent inner ear morphogenesis. *PloS one* Feb 1;5(2): e8981, 2010.

3. **Amundsen BH, Ericsson M, Seland JG, Pavlin T, Ellingsen O, and Brekken C.** A comparison of retrospectively self-gated magnetic resonance imaging and high-frequency echocardiography for characterization of left ventricular function in mice. In: *Lab Anim*. England, 2011, p. 31-37.

4. **Assmann G, Cullen P, and Schulte H.** The Munster Heart Study (PROCAM). Results of follow-up at 8 years. *European heart journal* 19 Suppl A: A2-11, 1998.

5. **Baker L, Meldrum KK, Wang M, Sankula R, Vanam R, Raiesdana A, Tsai B, Hile K, Brown JW, and Meldrum DR.** The role of estrogen in cardiovascular disease. In: *J Surg Res*. United States, 2003, p. 325-344.

6. **Del Rio T, Nishitani AM, Yu WM, and Goodrich LV.** In vivo analysis of Lrig genes reveals redundant and independent functions in the inner ear. In: *PLoS Genet*. United States, 2013;9(9):e1003824.

7. **Drayna D, Jarnagin AS, McLean J, Henzel W, Kohr W, Fielding C, and Lawn R.** Cloning and sequencing of human cholesteryl ester transfer protein cDNA. *Nature* 327: 632-634, 1987.

8. **Gassmann M, Casagranda F, Orioli D, Simon H, Lai C, Klein R, and Lemke G.** Aberrant neural and cardiac development in mice lacking the ErbB4 neuregulin receptor. *Nature* 378: 390-394, 1995.

9. **Guo D, Holmlund C, Henriksson R, and Hedman H.** The LRIG gene family has three vertebrate paralogs widely expressed in human and mouse tissues and a homolog in Ascidiacea. In: *Genomics*. United States: 2004 Elsevier Inc., 2004, p. 157-165.

10. **Guo D, Nilsson J, Haapasalo H, Raheem O, Bergenheim T, Hedman H, and Henriksson R.** Perinuclear leucine-rich repeats and immunoglobulin-like domain proteins (LRIG1-3) as prognostic indicators in astrocytic tumors. *Acta neuropathologica* 111: 238-246, 2006.

11. **Gur G, Rubin C, Katz M, Amit I, Citri A, Nilsson J, Amariglio N, Henriksson R, Rechavi G, Hedman H, Wides R, and Yarden Y.** LRIG1 restricts growth factor signaling by enhancing receptor ubiquitylation and degradation. In: *EMBO J*. England, 2004, p. 3270-3281.

12. **Hanahan D and Weinberg RA.** Hallmarks of cancer: the next generation. In: *Cell*. United States: 2011 Elsevier Inc, 2011, p. 646-674.

13. **Hedman H, Lindström AK, Tot T, Stendahl U, Henriksson R, and Hellberg D.** LRIG2 in contrast to LRIG1 predicts poor survival in early-stage squamous cell carcinoma of the uterine cervix. *Acta oncologica (Stockholm, Sweden)* 49: 812-815, 2010.

14. **Holmlund C, Haapasalo H, Yi W, Raheem O, Brännstrom T, Bragge H, Henriksson R, and Hedman H.** Cytoplasmic LRIG2 expression is associated with poor oligodendroglioma patient survival. In: *Neuropathology*. Australia, 2009, p. 242-247.

15. **Homma S, Shimada T, Hikake T, and Yaginuma H.** Expression pattern of LRR and Ig domain-containing protein (LRRIG protein) in the early mouse embryo. In: *Gene Expr Patterns*. Netherlands, 2009, p. 1-26.

16. **Jensen KB, Collins CA, Nascimento E, Tan DW, Frye M, Itami S, and Watt FM.** Lrig1 expression defines a distinct multipotent stem cell population in mammalian epidermis. In: *Cell Stem Cell*. United States, 2009, p. 427-439.

17. **Jensen KB and Watt FM.** Single-cell expression profiling of human epidermal stem and transit-amplifying cells: Lrig1 is a regulator of stem cell quiescence. In: *Proc Natl Acad Sci U S A*. United States, 2006, p. 11958-11963.

18. **Krig SR, Frietze S, Simion C, Miller JK, Fry WH, Rafidi H, Kotelawala L, Qi L, Griffith OL, Gray JW, Carraway KL, 3rd, and Sweeney C.** Lrig1 is an estrogen-regulated growth suppressor and correlates with longer relapse-free survival in ERalpha-positive breast cancer. In: *Mol Cancer Res*. United States, 2011, p. 1406-1417.

19. **Laederich MB, Funes-Duran M, Yen L, Ingalla E, Wu X, Carraway KL, 3rd, and Sweeney C.** The leucine-rich repeat protein LRIG1 is a negative regulator of ErbB family receptor tyrosine kinases. In: *J Biol Chem*. United States, 2004, p. 47050-47056.

20. **Ledda F, Bieraugel O, Fard SS, Vilar M, and Paratcha G.** Lrig1 is an endogenous inhibitor of Ret receptor tyrosine kinase activation, downstream signaling, and biological responses to GDNF. In: *J Neurosci*. United States, 2008, p. 39-49.

21. **Lee KF, Simon H, Chen H, Bates B, Hung MC, and Hauser C.** Requirement for neuregulin receptor erbB2 in neural and cardiac development. *Nature* 378: 394-398, 1995.

22. **Levin ER, Gardner DG, and Samson WK.** Natriuretic peptides. *The New England journal of medicine* 339: 321-328, 1998.

23. **Lindquist D, Näsman A, Tarjan M, Henriksson R, Tot T, Dalianis T, and Hedman H.** Expression of LRIG1 is associated with good prognosis and human papillomavirus status in oropharyngeal cancer. *British journal of cancer* 110: 1793-1800, 2014.

24. **Lindström AK, Ekman K, Stendahl U, Tot T, Henriksson R, Hedman H, and Hellberg D.** LRIG1 and squamous epithelial uterine cervical cancer: correlation to prognosis, other tumor markers, sex steroid hormones, and smoking. In: *Int J Gynecol Cancer*. United States, 2008, p. 312-317.

25. **Ma L, Yang J, Runesha HB, Tanaka T, Ferrucci L, Bandinelli S, and Da Y.** Genome-wide association analysis of total cholesterol and high-density lipoprotein cholesterol levels using the Framingham heart study data. In: *BMC Med Genet*. England, 2010, Apr 6;11:55.

26. **Muller S, Lindquist D, Kanter L, Flores-Staino C, Henriksson R, Hedman H, and Andersson S.** Expression of LRIG1 and LRIG3 correlates with human papillomavirus status and patient survival in cervical adenocarcinoma. *International journal of oncology* 42: 247-252, 2013.

27. **Nakamura T, Hamuro J, Takaishi M, Simmons S, Maruyama K, Zaffalon A, Bentley AJ, Kawasaki S, Nagata-Takaoka M, Fullwood NJ, Itami S, Sano S, Ishii M, Barrandon Y, and Kinoshita S.** LRIG1 inhibits STAT3-dependent inflammation to maintain corneal homeostasis. *The Journal of clinical investigation*, 2013, Jan;124(1):385-97.

28. **Nilsson J, Starefeldt A, Henriksson R, and Hedman H.** LRIG1 protein in human cells and tissues. *Cell and tissue research* 312: 65-71, 2003.

29. **Nilsson J, Vallbo C, Guo D, Golovleva I, Hallberg B, Henriksson R, and Hedman H.** Cloning, characterization, and expression of human LIG1. In: *Biochem Biophys Res Commun*. United States: 2001 Academic Press., 2001, p. 1155-1161.

30. **Parini P, Johansson L, Broijersen A, Angelin B, and Rudling M.** Lipoprotein profiles in plasma and interstitial fluid analyzed with an automated gel-filtration system. In: *Eur J Clin Invest*. England, 2006, p. 98-104.

31. **Perrone CE, Malloy VL, Orentreich DS, and Orentreich N.** Metabolic adaptations to methionine restriction that benefit health and lifespan in rodents. *Experimental gerontology* 48: 654-660, 2013.

32. **Powell AE, Wang Y, Li Y, Poulin EJ, Means AL, Washington MK, Higginbotham JN, Juchheim A, Prasad N, Levy SE, Guo Y, Shyr Y, Aronow BJ, Haigis**

KM, Franklin JL, and Coffey RJ. The pan-ErbB negative regulator Lrig1 is an intestinal stem cell marker that functions as a tumor suppressor. In: *Cell*. United States: 2012 Elsevier Inc, 2012, p. 146-158.

33. **Rafidi H, Mercado F, 3rd, Astudillo M, Fry WH, Saldana M, Carraway KL, 3rd, and Sweeney C.** Leucine-rich repeat and immunoglobulin domain-containing protein-1 (Lrig1) negative regulatory action toward ErbB receptor tyrosine kinases is opposed by leucine-rich repeat and immunoglobulin domain-containing protein 3 (Lrig3). In: *J Biol Chem*. United States, 2013, p. 21593-21605.

34. **Rondahl V, Holmlund C, Karlsson T, Wang B, Faraz M, Henriksson R, and Hedman H.** Lrig2-deficient mice are protected against PDGFB-induced glioma. In: *PLoS One*. United States, 2013, Sep 4;8(9):e73635..

35. **Rouam S, Moreau T, and Broet P.** Identifying common prognostic factors in genomic cancer studies: a novel index for censored outcomes. In: *BMC Bioinformatics*. England, 2010, Mar 24;11:150.

36. **Shattuck DL, Miller JK, Laederich M, Funes M, Petersen H, Carraway KL, 3rd, and Sweeney C.** LRIG1 is a novel negative regulator of the Met receptor and opposes Met and Her2 synergy. In: *Mol Cell Biol*. United States, 2007, p. 1934-1946.

37. **Smith NL, Felix JF, Morrison AC, Demissie S, Glazer NL, Loehr LR, Cupples LA, Dehghan A, Lumley T, Rosamond WD, Lieb W, Rivadeneira F, Bis JC, Folsom AR, Benjamin E, Aulchenko YS, Haritunians T, Couper D, Murabito J, Wang YA, Stricker BH, Gottdiener JS, Chang PP, Wang TJ, Rice KM, Hofman A, Heckbert SR, Fox ER, O'Donnell CJ, Uitterlinden AG, Rotter JI, Willerson JT, Levy D, van Duijn CM, Psaty BM, Witteman JC, Boerwinkle E, and Vasan RS.** Association of genome-wide variation with the risk of incident heart failure in adults of European and African ancestry: a prospective meta-analysis from the cohorts for heart and aging research in genomic

epidemiology (CHARGE) consortium. In: *Circ Cardiovasc Genet*. United States, 2010, p. 256-266.

38. **Suzuki Y, Miura H, Tanemura A, Kobayashi K, Kondoh G, Sano S, Ozawa K, Inui S, Nakata A, Takagi T, Tohyama M, Yoshikawa K, and Itami S.** Targeted disruption of LIG-1 gene results in psoriasiform epidermal hyperplasia. In: *FEBS Lett*. Netherlands, 2002, p. 67-71.

39. **Tanemura A, Nagasawa T, Inui S, and Itami S.** LRIG-1 provides a novel prognostic predictor in squamous cell carcinoma of the skin: immunohistochemical analysis for 38 cases. *Dermatologic surgery : official publication for American Society for Dermatologic Surgery [et al]* 31: 423-430, 2005.

40. **Telli ML, Hunt SA, Carlson RW, and Guardino AE.** Trastuzumab-related cardiotoxicity: calling into question the concept of reversibility. *Journal of clinical oncology : official journal of the American Society of Clinical Oncology* 25: 3525-3533, 2007.

41. **Thomasson M, Wang B, Hammarsten P, Dahlman A, Persson JL, Josefsson A, Stattin P, Granfors T, Egevad L, Henriksson R, Bergh A, and Hedman H.** LRIG1 and the liar paradox in prostate cancer: a study of the expression and clinical significance of LRIG1 in prostate cancer. *International journal of cancer Journal international du cancer* 128: 2843-2852, 2011.

42. **Wong VW, Stange DE, Page ME, Buczacki S, Wabik A, Itami S, van de Wetering M, Poulsom R, Wright NA, Trotter MW, Watt FM, Winton DJ, Clevers H, and Jensen KB.** Lrig1 controls intestinal stem-cell homeostasis by negative regulation of ErbB signalling. In: *Nat Cell Biol*. England, 2012, p. 401-408.

43. **Zhao H, Tanegashima K, Ro H, and Dawid IB.** Lrig3 regulates neural crest formation in Xenopus by modulating Fgf and Wnt signaling pathways. In: *Development*. England, 2008, p. 1283-1293.

551 **Legends to figures**

552

553 **Fig. 1** Schematic drawing of the wild-type, conditional, and disrupted *Lrig3* alleles and
554 Western blot confirmation of Lrig3 protein deficiency in *Lrig3* knock-out mice. (A) A PKG
555 neo-selection cassette was inserted downstream of the *Lrig3* exon 1. Exon 1 and the PKG
556 neo-cassette were flanked by *loxP* sites and were deleted together, in a single step, by mating
557 with OzCre mice, to generate the disrupted *Lrig3* allele. (B) Western blotting of the skin
558 lysates from wild-type (WT) and *Lrig3* knock-out (KO) mice using Lrig3 and actin
559 antibodies. The molecular weight markers are indicated

560

561 **Fig. 2** Van Gieson-stained sections from the left ventricle. (Left) Myocardium from the
562 female WT mouse with the lowest LVW/BW ratio. (Right) myocardium from the female KO
563 mouse with the highest LVW/BW ratio. Scale bar, 1 mm.

564

565 **Fig. 3** Myocardial gene expression in 12-month-old female mice. Gene expression in the left
566 ventricle was analyzed using quantitative real-time RT-PCR. The specific mRNA values were
567 normalized to the *Rn18s* level in the respective sample. The different groups ($n_{ko} = 9$; $n_{wt} =$
568 11) were compared using Student's *t*-test (*$p < 0.05$)

569

570 **Fig. 4** Plasma lipid levels in WT and *Lrig3* KO mice. Plasma samples from WT and KO mice
571 (n=9-12) were individually separated by SEC-HPLC gel filtration. The separated plasma was
572 subjected to triglyceride reagent (A and B) or cholesterol reagent (C and D). The groups were
573 compared using generalized estimating equations. The dashed lines represent the standard
574 error of the mean (SEM). The results are presented in Table 7.

575

Table 1. Body weight, tibia length, and organ weights of 12-month-old wild-type (WT) and *Lrig3*-deficient (KO) mice.

	Male		Female	
Weight	**WT (n=12)**	**KO (n=11)**	**WT (n=11)**	**KO (n=9)**
BW (g)	36.21±2.71	32.98±3.13*	27.98±3.41	24.61±2.20**
TL (mm)	17.78±0.22	17.41±0.26**	17.84±0.22	17.50±0.23*
HW (mg)	220±14	208±22	161±14	159±23
LVW (mg)	164±10	156±19	114±8	117±16
RVW (mg)	42±5	37±4*	32±4	30+±6
Atria (mg)	14.2±2.6	15.3±3.6	14.7±3.7	11.9±3.9
Spleen (mg)	86±13	91±17	107±22	124±7
Liver (g)	1.57±0.18	1.45±0.19	1.07±0.13	1.00±0.12
Lung (mg)	163±29	141±20*	130±16	124±17
HW/BW†	6.10±0.38	6.31±0.44	5.79±0.49	6.45±1.0
LVW/BW†	4.54±0.25	4.72±0.37	4.13±0.39	4.77±0.67*
RVW/BW†	1.17±0.17	1.12±0.12	1.14±0.11	1.23±0.26

Body weight (BW), tibia length (TL), heart weight (HW), left ventricle weight (LVW), right ventricle weight (RVW). † Ratio (10^-3), *p<0.05, **p<0.01.

583 **Table 2** Morphological measurments in tissue from 12 month old animals

Morphological mesurments		
	WT (n=10)	**KO (n=9)**
Collagen	+	+
Cardiomyocyte nuclei	23.04±2.55	25.17±4.68
Endothelial cell nuclei	3.4±0.57	3.56±0.7
Ratio	6.95±0.13	7.21±0.14

584 Morphological measurments in left ventricle sections of female mice. Collagen occurrence
585 were evaluated in Van Gieson-stained sections using a semiquantitative grading scale;
586 absent= 0, scarce=+, moderate=++ and abundant=+++. Nuclei were counted in 10 squares á
587 100x100 µm on Von Willebrand and Mayers HTX stained sections. The data are presented as
588 the mean (per square) ± SD. The groups were compared using Mann-Whitney *U*-test
589 (collagen) and Student's *t*-test.

590

591 **Table 3.** Heart rate measurements in 6- and 12-month-old mice.

Heart rate, heartbeats/min						
	WT	**KO**	**Male**		**Female**	
Age (months)	**n=23**	**n=20**	**WT (n=12)**	**KO (n=11)**	**WT (n=11)**	**KO (n=9)**
6	615±51	639±38	595±40	645±30**	635±56	631±46
12	656±33	662±38	652±35	659±22	660±32	665±53

592 The different groups (male WT/KO and female WT/KO) were compared using Student's *t*-

593 test (*p< 0.05, **p< 0.01). The data are presented as the mean ± SD.

594

595

596 **Table 4.** Blood pressure measurements in 6- and 12-month-old mice.

Blood pressure, mm Hg						
	WT	**KO**	**Male**		**Female**	
Age (months)	**n=23**	**n=20**	**WT (n=12)**	**KO (n=11)**	**WT (n=11)**	**KO (n=9)**
6	112.0±6.6	115.2±5.7	109.8±6.4	113.8±6.9	114.5±6.2	116.9±3.3
12	105.6±5.4	109.7±6.2*	107.1±4.4	110.7±6.8	104.0±6.2	108.4±5.5

597 The different groups (total WT/KO, male WT/KO and female WT/KO) were compared using

598 Student's *t*-test (*p< 0.05, **p< 0.01). The data are presented as mean ± SD.

599

Table 5. Echocardiographic measurements of the left ventricle for the male and female WT and KO mice at 6 months of age.

Echocardiography				
	Male		**Female**	
	WT (n=11)	**KO (n=10)**	**WT (n=10)**	**KO (n=9)**
HR (bpm)	474 ± 48	470 ± 56	438 ± 49	430 ± 33
FS (%)	26.6 ± 13	23.5 ± 7	26.5 ± 11	25.4 ± 5
EF (%)	44.9 ± 10	46.8 ± 12	44.4 ± 10	50.5 ± 7
SV (μL)	30.8 ± 11	25.4 ± 9	20.0 ± 6	22.3 ± 6
CO (mL/min)	14.4 ± 5	12.2 ± 5	8.9 ± 3	9.6 ± 3
EDV (μL)	77.6 ± 16	65.0 ± 17	55.8 ± 5	53.9 ± 7
AWd (mm)	0.38 ± 0.1	0.40 ± 0.1	0.39 ± 0.1	0.42 ± 0.1
LVIDd (mm)	4.48 ± 0.4	4.09 ± 0.3*	4.06 ± 0.1	3.85 ± 0.2**
PWd (mm)	0.79 ± 0.1	0.70 ± 0.2	0.72 ± 0.1	0.78 ± 0.1
AWs (mm)	0.51 ± 0.1	0.48 ± 0.1	0.49 ± 0.1	0.56 ± 0.1
LVIDs (mm)	3.45 ± 0.4	3.15 ± 0.4	3.10 ± 0.2	2.88 ± 0.3
PWs (mm)	1.05 ± 0.1	1.07 ± 0.1	0.88 ± 0.1	0.94 ± 0.2

Measurements using the parasternal long axis in B-mode or M-mode.

FS, fractional shortening; EF, ejection fraction; SV, stroke volume; CO, cardiac output; EDV, end-diastolic volume; AW, anterior wall thickness; LVID, left ventricular internal diameter; PW, posterior wall thickness; d, diastole; s, systole. The data are presented as mean ± SD. Student's *t*-test between the WT and KO mice and male and female mice (*$p < 0.05$ and **$p < 0.01$, respectively).

610 **Table 6**. Echocardiographic left ventricle measurements in the male and female and WT and

611 KO mice at 12 months of age.

Echocardiography				
	Male		**Female**	
	WT (n=10)	**KO (n=9)**	**WT (n=9)**	**KO (n=8)**
HR (bpm)	469 ± 51	453 ± 58	479 ± 37	469 ± 60
FS (%)	25.3 ± 5	24.9 ± 7	26.7 ± 6	26.3 ± 7
EF (%)	49.9 ± 8	48.9 ± 12	52.6 ± 8	51.7 ± 11
SV (µL)	30.9 ± 5	26.8 ± 7	21.8 ± 4	16.6 ± 3**
CO (mL/min)	14.4 ± 2	12.2 ± 5	10.4 ± 2	7.8 ± 2**
EDV (µL)	67.3 ± 11	57.7 ± 9	45.5 ± 5	42.4 ± 75
AWd (mm)	0.50 ± 0.1	0.44 ± 0.1	0.47 ± 0.1	0.55 ± 0.1
LVIDd (mm)	4.39 ± 0.4	4.22 ± 0.4	4.04 ± 0.1	3.85 ± 0.3
PWd (mm)	0.93 ± 0.1	0.92 ± 0.1	0.78 ± 0.1	0.89 ± 0.1*
AWs (mm)	0.66 ± 0.1	0.60 ± 0.1	0.61 ± 0.1	0.73 ± 0.1
LVIDs (mm)	3.29 ± 0.3	3.18 ± 0.4	2.96 ± 0.2	2.85 ± 0.4
PWs (mm)	1.19 ± 0.1	1.24 ± 0.1	0.96 ± 0.1	1.17 ± 0.2*

612 Measurements using the parasternal long axis in B-mode or M-mode.

613 FS, fractional shortening; EF, ejection fraction; SV, stroke volume; CO, cardiac output; EDV,

614 end-diastolic volume; AW, anterior wall thickness; LVID, left ventricular internal diameter;

615 PW, posterior wall thickness; d, diastole; s, systole. Student's *t*-test between WT and KO

616 males and females (*p< 0.05 and **p< 0.01, respectively).

617

618

Table 7. Plasma lipid levels in 12-month-old mice.

	Triglycerides			Cholesterol				
	VLDL	**IDL/LDL**	**Total**	**VLDL**	**LDL**	**HDL***	**Total**	**Glycerol ***
KO female (n=9)	**0.31**	**0.09**	**0.40**	**0.27**	**0.35**	**1.41**	**2.03**	**0.38**
WT female (n=11)	**0.40**	**0.07**	**0.47**	**0.48**	**0.33**	**1.64**	**2.44**	**0.38**
KO male (n=11)	**0.69**	**0.14**	**0.82**	**0.71**	**0.25**	**2.14**	**3.10**	**0.23***
WT male (n=11)	**0.71**	**0.13**	**0.84**	**0.73**	**0.26**	**2.36**	**3.34**	**0.34**

Fractional analysis of lipoprotein classes based on plasma separated by SEC-HPLC. The concentrations were estimated by calculating area under the curve (AUC), all values are mmol/L. The lipid profile of each group was compared using generalized estimating equations. Curves ± SEM are presented in figure 4. Differences in HDL and free glycerol were significant for the main effect genotype, but HDL was not for sex (*$p < 0.05$).

Table 8 Plasma insulin and glucose levels in 9-month-old mice

Insulin and Glucose levels						
	WT	**KO**	**Male**		**Female**	
	n=23	**n=19**	**WT (n=12)**	**KO (n=10)**	**WT(n=11)**	**KO (n=9)**
Insulin (ng/mL)	2.95±2.76	1.43±1.67*	4.10±3.08	2,26±2.00	1.70±0.86	0.52±0.14
Glucose (mmol/L)	6.54±3.13	5.95±0.86	5.72±2.55	6.14±0.42	7.44±3.57	5.73±1.16

Blood samples from 9 month old mice. The different groups (total WT/KO, male WT/KO and female WT/KO) were compared using One-way-ANOVA, Tukey's *post-hoc* test (*p< 0.05). The data are presented as the mean ± SD.

Sources of Funding

MH:

Umeå University and Västerbotten County Council (ALF) (VLL-163931, VLL-242061)

the Heart Foundation of Northern Sweden (2011) http://www.hjartfonden.com/

the Lion's Cancer Research Foundation at Umeå University (LP 11-1893) and

the Cancer Research Foundation in Northern Sweden, http://www.cancerforskningsfonden.se/

HH:

Umeå University and Västerbotten County Council (ALF) (VLL-292361)

Swedish Research Council (K2008-67X-15336-04-3) http://www.vr.se/

Swedish Cancer Society (13 0344) http://www.cancerfonden.se/

649 the Lion's Cancer Research Foundation at Umeå University (LP 11-1891, LP 04-1616)
650 and the Cancer Research Foundation in Northern Sweden,
651 http://www.cancerforskningsfonden.se/
652
653 ME and SN:
654 European Community's Seventh Framework Programme grants HEALTH-2013-2.4.2-
655 1/602936 (Project CarTarDis)
656
657 The funders had no role in study design, data collection and analysis, decision to
658 publish, or preparation of the manuscript
659
660
661

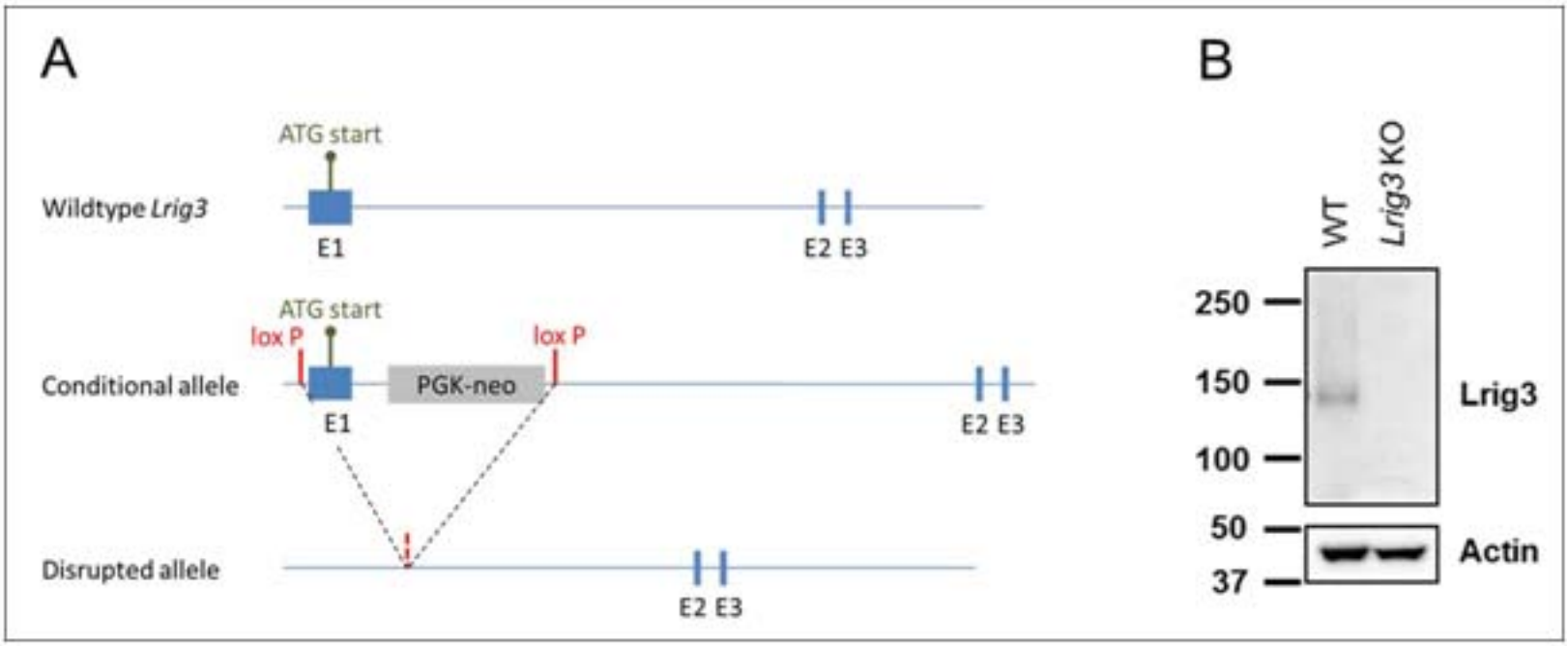
A
ATG start
Wildtype Lrig3
E1
E2 E3
ATG start
lox P
lox P
Conditional allele
PGK-neo
E1
E2 E3
Disrupted allele
E2 E3
B
WT
Lrig3 KO
250
150
100
50
37
Lrig3
Actin

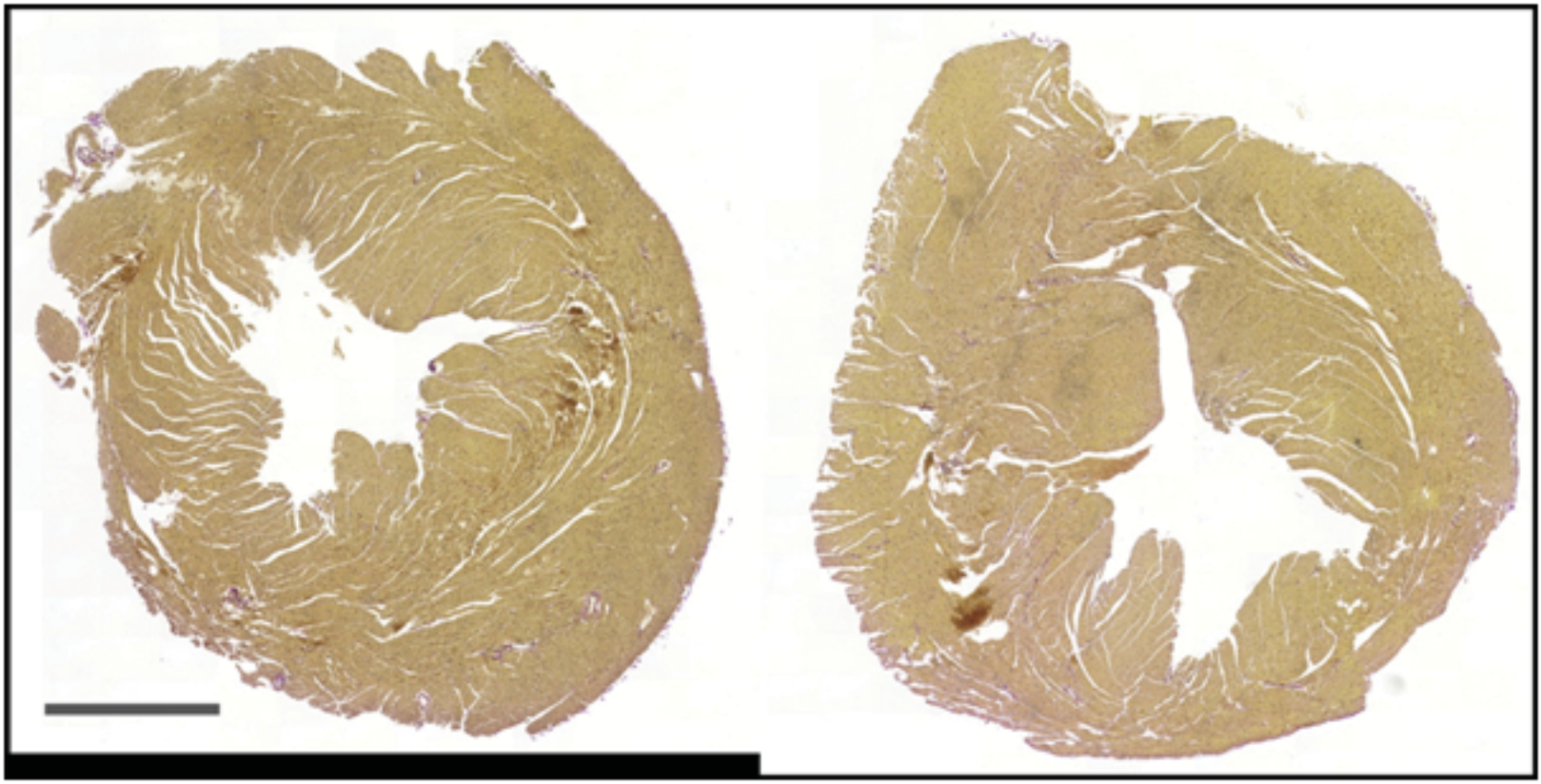

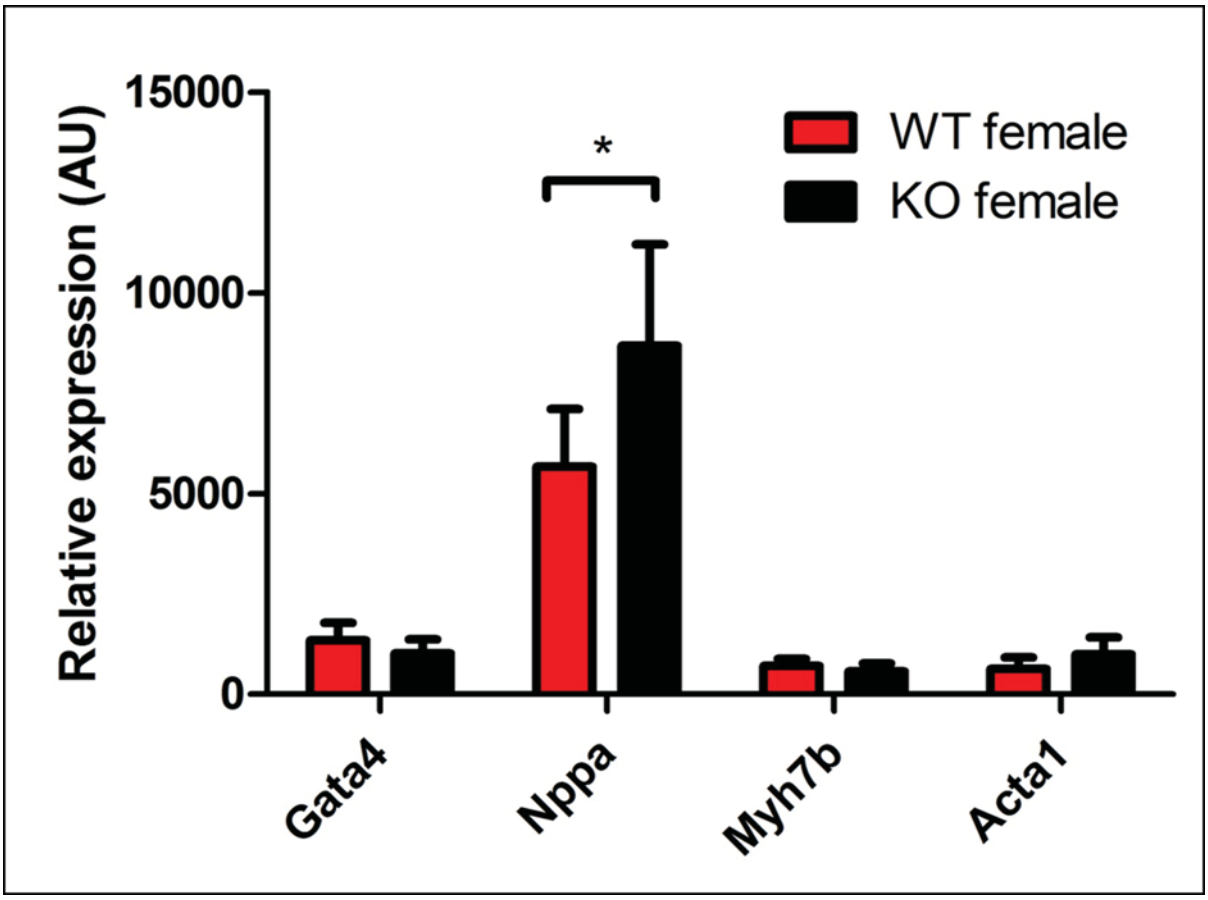
Relative expression (AU)
15000
10000
5000
0
*
WT female
KO female
Gata4
Nppa
Myh7b
Acta1

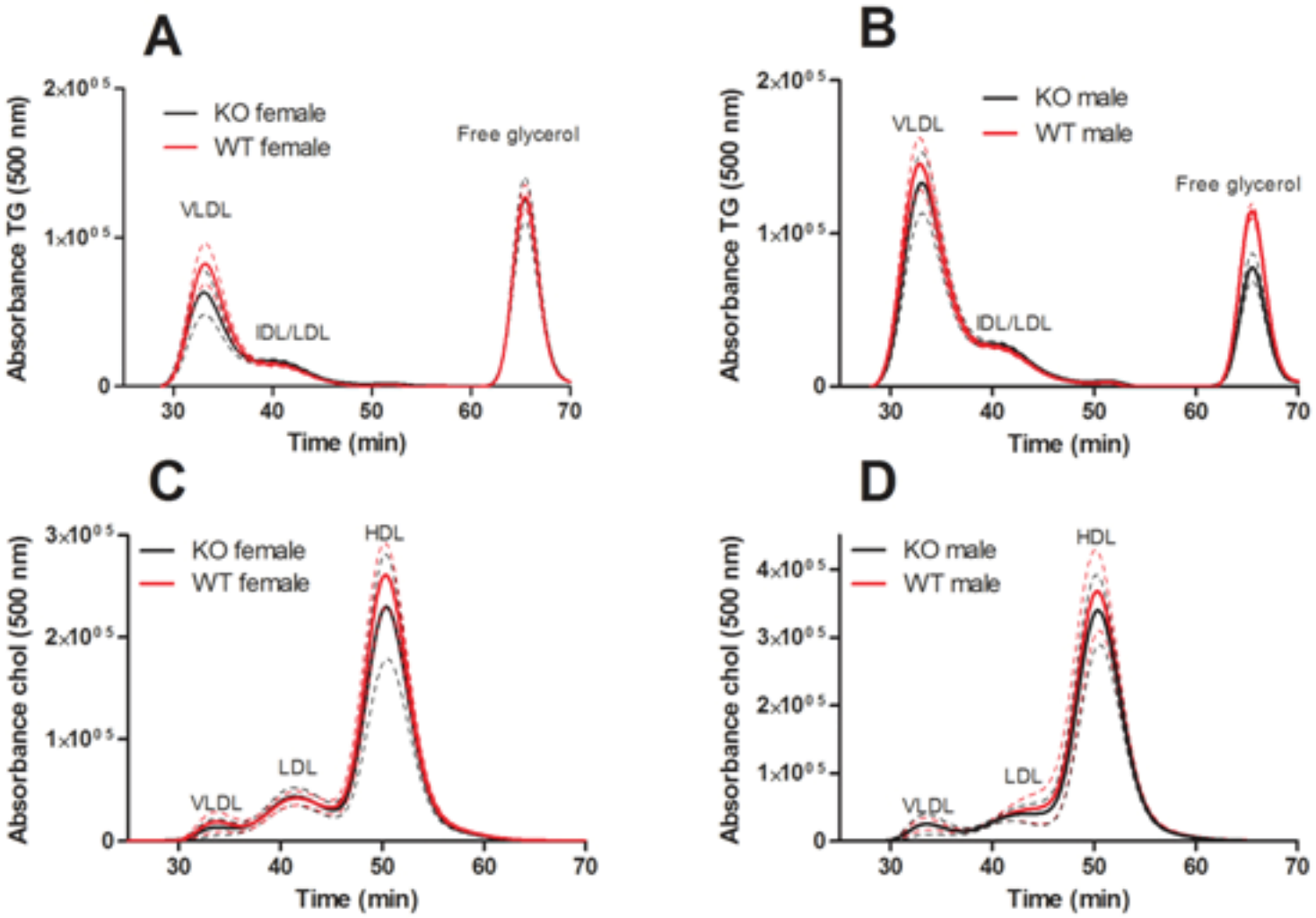
A
KO female
WT female
Free glycerol
VLDL
IDL/LDL
Absorbance TG (500 nm)
Time (min)
B
KO male
WT male
VLDL
Free glycerol
IDL/LDL
Absorbance TG (500 nm)
Time (min)
C
KO female
WT female
HDL
LDL
VLDL
Absorbance chol (500 nm)
Time (min)
D
KO male
WT male
HDL
LDL
VLDL
Absorbance chol (500 nm)
Time (min)